RSC Advances

ROYAL SOCIETY OF CHEMISTRY

www.rsc.org/advances

Excited-state dynamics and electron transfer process of 1,3,5-triamino-2,4,6-trinitrobenzene

Genbai Chu[1], Feng Lu[1], Jianting Xin[1], Tao Xi[1], Min Shui[1*], Weihua He,[1] Yuqiu Gu[1*], Ying Xiong[2], Kemei Cheng[2], Tao Xu[2]

[1]*Science and Technology on Plasma Physics Laboratory, Research Center of Laser Fusion, China Academy of Engineering Physics, 621900, P. R. China*

[2]*Institute of Chemical Materials, China Academy of Engineering Physics, Mianyang 621900, P. R. China*

Corresponding authors:shm@caep.cn; yqgu@caep.cn.

Excited-state dynamics and electron transfer processes of 1,3,5-triamino-2,4,6-trinitrobenzene

Abstract: Insights into the excited-state dynamics and electron transfer processes of nitroexplosives offer an efficient tool forunravelling ultrafast and complex detonation physics. In this work, the excited state dynamics and electron transfer processes of 1,3,5-triamino-2,4,6-trinitrobenzene (TATB) were studied using femtosecond transient absorption spectroscopy and time-dependent density functional theory. The de-excitationof TATB after excitation at 400 nm involves an equilibrium between the vibrationally hot S_1 (S_1^*) and S_1 states, with lifetimes of 0.64 and 6 ps, respectively. After vertical excitation,the electrondensity is transferred from the C-ring and NH_2 group to NO_2 groups. The excitation energy activates the nitro groups, andenergy is redistributed via theirnuclear motion.The relaxation of the initial S_1^* state shows an apparent structural change occurring at one activated nitro group, which becomesfurther twisted from the planar benzene ring and relaxes to the S_1–T_1 conical intersection. The T_1 state is populated via the minimal intersystem crossing through the S_1–T_1 intersection. The nitro group charge transfer process is then explored following the ultrafast structural change. This study advances our understanding of photo-initiated reactions as well as the ignition of energetic materials.

Introduction

Molecules exhibit different behaviours in the excited state compared to the ground state[1-4].As a matter of general interest, ultrafast and complex photo-initiated reactions can be mechanistically probed by effectively exploitingultrafast excited-state dynamics and electron transfer processes[5-9].Excited-state behaviour has been extensively studied using ultrafast pump-probe spectroscopy[10, 11]. Detailed investigations of the electronic, structural, geometric, and chemical changes that take place when a molecule is promoted to the excited state can enable us to understandthe inherent physical and chemical processes that ensue[12].

Energetic materials (EMs) areorganic compounds with substantial amounts of stored chemical energy that can be released under extreme conditions, such as exposure to photons, shock, or rapid heating[13, 14]. EMs, which include fuels and explosives, are widely utilized in many fields; however, their useful energy conversion featureshave associated problems of safety, reliability, and application[15]. On the molecular level, very little is known about the dynamic responses of these materials. For example, electronic excitation plays a crucial role in the energy conversion processes of EMs. Insights into the excited-state dynamics of these materialsand their electron transferbehaviours would potentially allow us to unravel these inherent mechanisms, and would also have implications for the behaviour of other nitro derivatives.

Among EMs, nitroexplosives constitute the major class.The introduction of a nitro group into a molecule greatly changes its photo-physical behaviour, and can impact the molecular stability and impact sensitivity[16, 17]. The electronically excited state of a nitro-containing species undergoes ultrafast intersystem crossingand exhibits a high quantum yield of the triplet state. For example, de-excitationof the nitrostilbene derivative,2,2′,4,4′,6,6′-hexanitrostilbene (HNS),was revealed to involve a majorchange from the $S_1$to the T_1 state with a lifetime of 6 ps[18]. It isessential to understand the photo-induced behaviour of nitro-containing species. As a type of nitro explosive,

1,3,5-triamino-2,4,6-trinitrobenzene (TATB) is of particular interestbecause,although it is relatively stable to external stimuli such as heat, impact, and shock[19-21],it is a photo-sensitive EM that exhibitscolour changes under light irradiation[22]. A study of the evolution of the excited states and photo-induced electron transfer of TATB is crucial to understanding the importance of nitro groups and EMs ignition.

In this work, we present an experimental and theoretical investigation of the excited-state dynamics and electron transfer processes of TATB. The initial S_1^* state of TATB and its evolution into the S_1 state with lifetimes of 0.64 and 6 ps, respectively, were observed using femtosecond transient absorption spectroscopy at an excitation wavelength of 400 nm. The structural relaxation that occurs as the S_1^* state evolves to the S_1 state, with the apparent structural change occurring at a nitro group, was investigated using the time-dependent density functional theory (TD-DFT) method at theB3LYP/6-311++G(d,p) level.An S_1–T_1 conical intersection was suggested to enhance the efficiency of intersystem crossing. The electron distribution was also evaluatedin order to explain the structural change. Ultrafast nitro group charge transfer (Q_{nitro}),which occurssubsequent to the structural changes, was also explored. The study advances our understanding of ultrafast electron transfer in EMs.

Experimental and theoretical section

TATB powder (purity > 99.5%) was synthesized at the Institute of Chemical Materials at the China Academy of Engineering Physics. For the transient absorption spectroscopy experiments, the concentration of TATB in dimethyl sulfoxide (DMSO, 99% purity) was 1 mmol/L. The solution was flowed at room temperature using a slow-flow device to avoid decomposition induced by the ultraviolet excitation at 400 nm.

The typical equipment used to obtain transient absorption spectra has been described previously[11, 23]. Briefly, a laser system generates fundamental femtosecond pulses at 800 nm, with a pulse duration of 35 fs, energy per pulse of 1 mJ, and repetition rate of 1 kHz. As the pump beam, the third harmonics (266 nm) of the fundamental pulses were attenuated to ~5 μJ. The white-light-continuum (WLC) pulses from a CaF_2 crystal were used as the probe beam, with a spectral range of 440–640 nm. The pump-probe pulses were organized as follows: the pump-pulse beam was lead and collimated onto the sample cell (1 mm optical pathlength). The probe-pulse beam passed through an optical delay line, and then was split into two parts by a metallic beamsplitter. One part was collimated and overlapped with the pump-pulse in the sample cell. The other was collimated into the sample cell at a different spot as a reference signal,to improve sensitivity. The polarization plane of the probe pulses was rotated by a λ/2 plate, and a magic angle (54.7°) configuration between the pump and probe pulses was adopted in all the measurements. Given the speed of light (3×10^8 m/s), the delay time was varied up to 500 ps with a minimum interval of 2.08 fs. The probe-pulse beam was dispersed by a grating inside the spectrometer (Princeton, SpectraPro 2500i) and detected by a two-dimensional CCD detector (PI-MAX,1024× 256 pixel array). On the CCD surface,twoimage signal stripes were formed, one from the probe and the other from the reference. Each of these signals was sent to a computer through a 16-bit analog-to-digital converter (ADC). The data acquisition and experiment control were performed via theLabView program. A low noise level (<2 mOD) could be achieved by averaging approximately 1600 pulses. The instrumental response of the system was determined to be ~180 fs by cross-section measurements between the pump and probe pulses. The chirp of the

WLC was measured at the position of the sample cell byusing the optical Kerr effect of the solvent; this value was used to correct the dispersion of the relative delay time in the time-resolved data. The stimulated emission, ground state bleach, and dark response were eliminated bylogical collections, by the use of two shutters. The absorption of excited states, transient products, and long-lived molecular states such as triplet state would acquire $\Delta A>0$, while the bleaching of the ground state absorption and stimulated emission are obtained for $\Delta A<0$. Therefore, the spectral changes could be sometimes complicated and required special methods to accurately analyse the time-resolved data.

The TD-DFT method at the B3LYP/6-311++g(d,p) level was employed to calculate the vertical excitation energies and optimize the structures in the ground (S_0)and first singlet excited (S_1) states[24]. The first triplet excited (T_1) state was also obtained at this level by changing the spin multiplicity. The natural population analysis (NPA) charge was utilized in this study. The absorption spectra were obtained at the wb97xd/cc-pVTZ level. The Kohn-Sham orbitals, orbital energies, and density-of-states (DOS) spectra were also obtained at this level, to avoid the effects of a diffuse basis function. All the calculations were performed using Gaussian 09 software[25]. Although TD-DFT was not as accurate as multi-configuration methodssuch as the complete-active-space self-consistent field (CASSCF) method, TD-DFT provided reliable results for the related states of this molecule, according to our tests, because it had no multi-configuration effects. It should be pointed out that the TD-B3LYP method is not well suited for searching for an intersection point, and the CASSCF method is too expensive for performing such calculations. The molecular orbitals, electron distributions, and DOS spectra were obtained usinga wave function analyser (Multi-wfn)[26].

Experimental and theoretical results

1. Kohn-Sham orbitals, DOS, and steady-state absorption spectra

The structure of TATB in the S_0 state (TA-S_0) and the highest occupiedand lowest unoccupied molecular orbitals (HOMOs and LUMOs, respectively) are shown in Fig. 1. The electron density in HOMO-2 is mainly distributed between C5 and N16, and is mainly distributed among C1, C3, and N19 in HOMO-1. Both orbitals exhibit non-bonding (n) character. HOMO-1 and HOMO-2 have the same energy of −8.99 eV. The electron density in LUMO-1, which shows anti-bonding(π^*) character, is distributed equally among the three NO_2 groups, whereas the electron density in LUMO-2 is distributed primarily and symmetricallybetween one NO_2 and NH_2 group[27].LUMO-1 and LUMO-2 have energies of −0.90 and −0.67 eV, respectively. From the orbital analysis, it can be inferred that the low-lying excited states are accessed through HOMOs → LUMOs transitions that can be assigned as $n\rightarrow\pi^*$ transitions.

The total, partial, and overlap density-of-states (TDOS, PDOS, and OPDOS) for TATB are shown in Fig. 2. In the TDOS map, each discrete vertical line corresponds to a molecular orbital (MO). The curve for the TDOS was simulated based on the distribution of MO energy levels. From the PDOS, it is clear that the nitro groups contribute the most to the valence MOs. In the range from −10.0 to −7.5 eV, there are comparable contributions from the C-ring and NH_2 groups. However, the contributions arereduced to a low level in the range from−3.0 to 0.0 eV. The OPDOS is negative in the −3.0–0.0 eV range, which indicates the anti-bonding orbitals between the NO_2 groups andother moieties. The DOS curves also show that the low-lying excitation process can be assigned as $ann\rightarrow\pi^*$ transition.

In the experimentally obtained steady-state absorption spectrum of TATB in DMSO, there is a wide band centred at 357 nm, which extends to the 450 nm range[28] (Fig. 3). The extension of the experimental absorptionresults from the "hot band" effect that occurs at room temperature and weak interactions in solution, such as intramolecular and intermolecular H bonds. The band is centred at 301 nm in the calculated spectrum, which is lower than that observed experimentally. This may be explained by an overestimation of the excitation energy by the TD-DFT method. However, this discrepancy does not affect the general discussion in this work. From the orbital information above, the peak can be assigned as ann→π^* transition (S_1 state),which is Franck-Condon-state-accessible from the vibrational ground state configuration. At400 nm, thestrong absorption efficiencyindicates the vertical excitation from the contribution of MO pairs of the low-lying transition dipole moment. Thus, from the calculations in this paper, the ultraviolet excitation at 400 nm (3.10 eV) suggests that TATB molecules are vertically excited to the S_1 surface from the vibrational ground state.

2. Transient absorption spectra and the dynamic process

The evolution-associated difference spectra (EADS, Fig. 4)were obtainedfrom a global analysis of the transient absorption experiments for TATB. The background level is shown at a time delay of −0.4 ps before the overlap of the pump-probe pulse. The first EADS evolves into the second one in 0.1 ps, which is characterized by a strong transient absorption. This corresponds to the population of the initial excited state, which can be assigned as the S_1^* state. In addition, there are two peaks centred at 470 and 600 nm, respectively, indicative of the two absorption bands of the S_1^* state. The evolution of the third EADS takes place in 4 ps, andcorresponds to the decrease of the excited state absorption at 600 nm. Moreover, a peak shift from 470to 450 nm is observed, which can be assigned to the vibrational cooling of the S_1^* state to the S_1 state. The fourth EADS appears with the decay of the S_1 state to the background level in 20 ps.

Dynamics tracesrecorded at 600 nm (upper panel) and 450 nm (lower panel) are presented in Figs. 4b and4c, respectively. Here, the lifetimes were fitted with a convolution of a Gaussian-type instrumental response function and an exponential decay rate. The obtained lifetimes for the S_1^* and S_1 states are 0.64 and 6.0 ps, respectively, from the best fits of the two curves. The former value is in agreement with those observed for the S_1^*→S_1 transitions of HNS[18] (0.8 ps),carotenoids[11] (0.9 ps), and *trans*-4-aminoazobeneze[23] (0.7 ps). The S_1 state lifetimeaccords wellwith that observed for the S_1→T_1 transition of HNS[18](6 ps) and the S_1 → S^*transition of *o*-nitroaniline[29] (6.4 ps).

3. Structures, orbital information, and potential energy surfaces of excited states

Starting from TA-S_0, the low-lying excited states are accessed mainly by the vertical transitions HOMOs →LUMOs, as shown in Fig. 1. The low-lying vertical excitation energy to the S_1 surface wascalculated as 3.67 eV,without any geometrical change[22]. After its vertical excitation, the electron density is transferred from the C-ring and NH_2 groups to a NO_2 group, as shown in Figs. 2. There is a major contribution from LUMO-1 to the dipole moment, in addition to some contribution from LUMO-2. The subsequent transitions of LUMO-1 proceed via vertical excitations to higher unoccupied molecular orbitalssuch as LUMO-4 and LUMO-6 (Fig. 5). From the electron distribution spectra, it can be deduced that bothof these transitions are highly possible. The electron can be re-excited to higher π^* and σ^* orbitals, which is indicated by the two absorption peaks at 470 and 600 nm in the transient absorption spectra in Fig. 4.

The initial excitation energy, aftermaking the NO_2 groups active, is redistributed via the nuclear

motionof the active nitro group (i.e. relaxation). Relative to TA-S_0, the C(5)–N(10) bond and two N(10)–O(11,12) bonds of TA-$S_1$are lengthened by about 0.04 Å, respectively. Also, the energy of TA-S_1 in the S_1 state is 3.42 eV, a reduction of 0.25 eV. The apparent change is suggested to be due primarily the vibrational cooling of the $v_s(NO_2)$ mode. The electron density is mainly distributed in LUMO-1 of the active nitro group in TA-S_1, which is much different from that of TA-S_0; this further indicates an electron has been transferred into the active nitro group in the relaxation process. Thus, it is still feasible that the electron can be re-excited to LUMO-6 from LUMO-1, based on the electron distribution in Fig. 5. However,the re-excitation of LUMO-1to LUMO-4 is infeasible because of the electron transfer in the relaxation process. Referring to the EADS in Fig. 4,the feasible re-excitation corresponds to the blue shift of the peak at 470to 450 nm, while the infeasible re-excitation corresponds to the disappearance of the absorption peak at 600 nm.

The bond of the active NO_2 group, which exhibits π^* character, becomes further twisted from the planar benzene ring.After optimization, TA-S_1' in the S_1 state exhibits a dihedral C(4)C(5)N(10)O(12) twist of 69.7° and a dihedral C(6)C(5)N(10)O(11) twist of 104°.The electron density is mainly distributed in the NO_2 group with the deviated structure in Fig. 6, as LUMO-1 of TA-S_1'. The energy of the LUMO is reduced to −2.36 eV, and the energy of TA-S_1' in the S_1 state is greatly reduced to2.25 eV. In the meantime, the energy of TA-S_1' in the T_1 state is calculated as 2.43 eV, slightly higher than that in the S_1 state. This means that the TA-S_1' structure is close to the point of the S_1–T_1 conical intersection, which is suggested to enhance the efficiency of intersystem crossing and greatly reduce the lifetime of the transition[30]. Thus, the T_1 state can be easily populated via a minimal intersystem crossing from the S_1 state. The TA-T_1structure was also optimized, and displayed the electron distribution in the deviated NO_2 group, in good agreement with the foregoing discussion. The dihedral C(4)C(5)N(10)O(12) twists to 46.9° and the dihedral C(6)C(5)N(10)O(11) twists to 84.2°, such thatthatO(11) is nearly perpendicular to the benzene ring. The energy of TA-T_1 in the T_1 state is 2.30 eV, much lower than that on the S_1 surface.

To summarize, the NO_2 groups in TATB are activated after vertical excitation to the S_1 state, which show their π^* bond character. Then, they are relaxed via the vibrational cooling of one active nitro group, leading to TA-S_1 in the S_1 state. The nitro group is further twisted from the planar benzene ring so as to approach the S_1–T_1 conical intersection. The T_1 state is then populated viaminimal intersystem crossing. Overall, the electron distribution spectra provide a new insight into the de-excitation process.

4. Q_{nitro} transfer process

One nitro group of TATB becomes the active site aftervertical excitation. On basis of the foregoing discussion, theQ_{nitro} transfer process is summarized in Table 1.

The initial Q_{nitro}values at the three sites are 0.397, 0.397, and 0.397 (−e), respectively. Afterexcitation, they increase to0.459, 0.459, and 0.459 (−e), respectively, indicating charge transfer from the benzene ring to the three nitro groups. In the relaxation process of the initial excited state, Q_{nitro} is transferred from the other two sites to Site 1. The overall Q_{nitro} does not change significantly in the redistribution process, but Q_{nitro} at Site 1 increases to as high as 0.727 (−e). It is noted that the Q_{nitro} distribution at the three sites of TA-S_1 in the S_1 state is different from that in the S_0 state, mainly at Site 1. This result comports with the deviation of the NO_2 group taking place on the S_1 rather than the S_0 surface.Subsequently, the Q_{nitro} transfer process involves mainly the decrease of Q_{nitro} at Site 1 via deviation of the NO_2 group. The Q_{nitro} at Site 1 decreases

to 0.645 (−e) in the T_1 state of TA-S_1', rather than0.887 (−e) in the S_1 state. Furthermore, the Q_{nitro} at Site 1 decreases to 0.598 (−e) in succession without significant change at the other two sites.

Overall, the ultrafast Q_{nitro} transfer process involves a) an initial increase afterexcitation, then b) redistribution from the first two sites to Site 1, and c) a decrease at Site 1 via the deviation of the NO_2 group. The Q_{nitro} transfer process is also in accord with the NO_2 group deviation on the S_1 surface rather than on the S_0 surface. This study of the dynamic response of EMs upon excitation shows potential application for the exploration of EMs under other extreme conditions.

Discussion

1. Assignment of the $S_1 \rightarrow T_1$ transition and de-excitation process

The de-excitationof a relaxed S_1 state usually proceeds via fluorescence emission, non-radiative transition to the ground state, or intersystem crossing to the T_1 state. In this work, the fourth EADS inthe transient absorption spectra decayed to the background levelwithout providing any additional information about the de-excitation process. Therefore, we must analyse the transition according to the following information: first, TATB is a photosensitive EM which undergoes colourchanges from yellow to green or darker under light irradiation/photolysis,which has been attributed to the formation of a long-lived radical in the T_1 state[22]; andsecond,intersystem crossing to the T_1 state is likely to happen in this case.By way of explanation, one may consider that the conical intersection is probably close to TA-S_1', as discussed in the previous section. The Kohn-Sham orbitals, electron distribution, and orbital energies are in good agreement with this interpretation. Alternatively, a previous study using nanosecond transient absorption spectroscopy under N_2 and O_2 conditions showed that the T_1 state absorption occurs at wavelengths of 340 and 410 nm, respectively[31]. Unfortunately, those peaks are beyond the present experimental range.Ultimately,the lifetime of the singlet excited state of the nitro-substituted species is greatly reduced and the quantum yield of the triplet state is relatively high[32, 33]. TATB exhibits behaviour similar to HNS, which undergoes a major $S_1 \rightarrow T_1$ intersystem crossing.Some reports show that there is an intermediate state in the intersystem crossing, when the participating singlet and triplet states are composed of essentially the same orbitals in terms of the El-Sayed rule[29]. On the basis of the foregoing arguments, it would be reasonable to assign the decay of the relaxed S_1 state to the $S_1 \rightarrow T_1$ transition in this work.

2. The importance of the nitro group in nitro explosives

The nitro group has been shown herein to be an important factor in the excited-state dynamics and electron transfer in TATB, and its influence can probably be extrapolated as a general rule for nitro explosives[34]. The lone pair electrons in the nitro group make an essential contribution to the HOMOs, and the anti-bonding π orbital of the nitro group contributes the most to the LUMOs. When the moleculesuffers an external stimulus, an electron is excited and transferred into a low-lying MO of the nitro group via the excitation energy. The nitro group is activated by the π^* bonding character, which can be readily observed in the electron distribution spectra. The active nitro group is then perturbed in some typical way, such as through vibrational cooling followed by deviation from coplanarity with the benzene ring.The observed results are in good agreement with the major NO product obtained from the dissociation of EMs in the excited state[15]. The overall process typically occurs on the picosecond or even femtosecond time scale. The extra energy is converted into thermal energy via vibrational and translational motion, which is further transferred into the surroundings via intermolecular interactions.

The nitro group plays an important role in the initial reactions of nitro explosives. The excitation and relaxation processesthat take place with other explosives such as RDX, HMX, CL20, and PETN have also been investigated[34]. These exhibitsimilar behaviours, and their impact sensitivity was found to be related to the excitation energy of the relaxed structure. Consequently, other characteristics also influence the impact sensitivity of these EMs, including their crystal, surface, and interfacial structures. These characteristics should clearly be considered infuture work.

3. Implications for the photo-behaviour of nitroderivatives

The anti-bonding π orbital of the nitro group is large, conjugated with the aromatic ring, and is relatively low in energy. Under light irradiation,electronic excitation couples the excitation energy into the low-lying LUMOs, such as those with π* bonding character in a nitro group.The nitro group is activated by the excitation energy and then relaxes by a typical pathway, such as vibrational cooling orstructural deviation. This process is indicated bythe greatly reduced lifetime of the singlet excited state of nitro-substituted speciesand the relatively high quantum yield of the triplet state[24, 32, 33, 35]. Such processes can be observed via the ultrafast pump-probe technique.

Importantly, there are several differences between nitroderivatives and nitroexplosives. Nitroexplosives usually have a symmetrical structurewith many nitro groups. The influence of the nitro groupson the photo-physical behaviour of the materials is distinct and clear. Nitroderivatives have fewer nitro groups thannitroexplosives. In the low-lying unoccupied orbitals, the nitro group can be conjugated with other groups, such as aromatic rings and NH_2. Such nitro groups exhibit distinct photo-physical behaviours depending on their geometrical arrangement and electron distribution[24, 35, 36].

Thus, the introduction of a nitro group into a molecule greatly changes the photo-physical behaviour of the derivative, and studies of theexcited-state dynamics and electrontransfer processes caneffectively serveto unravel the ultrafast and inherently complex changes that occur.

Conclusions

The combination of femtosecond transient absorption spectroscopy and the TD-DFT method in this work offers a distinctive approach to studying ultrafast excited-state dynamics and electrontransfer processes, especially the changes in the π* bonding character of the nitro group in nitro explosives.

The initial S_1^* state was observed at an excitation of 400 nm, with two peaks centred at 470 and 600 nm. This state evolved into the S_1 state, with a peak at 450 nm from EADS. The lifetimes of the two states were found to be 0.64and 6 ps, respectively. The electron densitywas transferred from the C-ring and NH_2 groups to the NO_2 groups aftervertical excitation. The excitation energy activatedthe nitro groups and was then redistributed via their nuclear motion. The structural relaxation of the initial S_1^* state revealed that the electron density was mainly distributed in the activated nitro group. Then, the active nitro group wasfurther deviated from coplanarity with the benzene ring and relaxed to the S_1–T_1 conical intersection point. The T_1 state was suggested to be populated viaminimal intersystem crossing through the S_1–T_1 intersection. The electron distribution spectra provided a new insight into the de-excitation process. This study advances our understanding of photon-initiated reactions and EM ignition processes.

References

1. N. Tamai and H. Miyasaka, *Chem. Rev.*, 2000, **100**, 1875.

2. J. Ma, J. Zhao, P. Yang, D. Huang, C. Zhang and Q. Li, *Chem. Comm.*, 2012, **48**, 9720.
3. D. Achey, E. C. Brigham, B. N. DiMarco and G. J. Meyer, *Chem. Comm.*, 2014, **50**, 13304.
4. G. A. Parada, T. F. Markle, S. D. Glover, L. Hammarstrom, S. Ott and B. Zietz, *Chemistry*, 2015, **21**, 6362.
5. M. H. Kim, L. Shen, H. Tao, T. J. Martinez and A. G. Suits, *Science*, 2007, **315**, 1561.
6. N. E. Levinger and L. A. Swafford, *Annu. Rev. Phys. Chem.*, 2009, **60**, 385.
7. M. J. Jordan and S. H. Kable, *Science*, 2012, **335**, 1054.
8. R. A. Mathies, *Nat. Chem.*, 2015, **7**, 945.
9. I. V. Rubtsov, *Nat. Chem.*, 2015, **7**, 683.
10. C. L. Evans and X. S. Xie, *Annu. Rev. Anal. Chem.*, 2008, **1**, 883.
11. R. Berera, R. van Grondelle and J. T. Kennis, *Photosynth. Res.*, 2009, **101**, 105.
12. C. Adamo and D. Jacquemin, *Chem. Soc. Rev.*, 2013, **42**, 845.
13. J. E. Field, *Acc. Chem. Res.*, 1992, **25**, 489.
14. N. C. Dang, C. A. Bolme, D. S. Moore and S. D. McGrane, *J. Phys. Chem. A*, 2012, **116**, 10301.
15. A. Bhattacharya, Y. Guo and E. R. Bernstein, *Acc. Chem. Res.*, 2010, **43**, 1476.
16. C. Zhang, *J. Hazard. Mater.*, 2009, **161**, 21-28.
17. C. Zhang, Y. Ma and D. Jiang, *J. Mol. Model.*, 2012, **18**, 4831.
18. G. Chu, M. Shui, Y. Xiong, J. Yi, K. Cheng, T. Xu, J. Xin and Y. Gu, *RSC Adv.*, 2014, **4**, 60382.
19. C. J. Wu, L. H. Yang, L. E. Fried, J. Quenneville and T. J. Martinez, *Phys. Rev. B*, 2003, **67**, 235101.
20. O. U. Ojeda and T. Cagin, *J.Phys.Chem. B*, 2011, **115**, 12085.
21. C. Zhang, B. Kang, X. Cao and B. Xiang, *J.Mol.Model.,* 2012, **18**, 2247.
22. Y. Xiong, F. Zhong, T. Xu, K. Cheng, *J.Phys.Chem. A*, 2014, **18**, 6858.
23. Y. p. Wang, S. Zhang, S. m. Sun, K. Liu and B. Zhang, *Chin. J. Chem. Phys.*, 2013, **26**, 651.
24. R. A. Vogt, C. Reichardt and C. E. Crespo-Hernandez, *J. Phys. Chem. A*, 2013, **117**, 6580.
25. M. J. T. Frisch, G. W.; Schlegel, H. B.; Scuseria, G. E.; Robb, M. A.; Cheeseman, J. R.; Scalmani, G.; Barone, V.; Mennucci, B.; Petersson, G. A.; Nakatsuji, H.; Caricato, M.; Li, X.; Hratchian, H. P.; Izmaylov, A. F.; Bloino, J.; Zheng, G.; Sonnenberg, J. L.; Hada, M.; Ehara, M.; Toyota, K.; Fukuda, R.; Hasegawa, J.; Ishida, M.; Nakajima, T.; Honda, Y.; Kitao, O.; Nakai, H.; Vreven, T.; Montgomery, J. A.; Jr.; Peralta, J. E.; Ogliaro, F.; Bearpark, M.; Heyd, J. J.; Brothers, E.; Kudin, K. N.; Staroverov, V. N.; Keith, T.; Kobayashi, R.; Normand, J.; Raghavachari, K.; Rendell, A.; Burant, J. C.; Iyengar, S. S.; Tomasi, J.; Cossi, M.; Rega, N.; Millam, J. M.; Klene, M.; Knox, J. E.; Cross, J. B.; Bakken, V.; Adamo, C.; Jaramillo, J.; Gomperts, R.; Stratmann, R. E.; Yazyev, O.; Austin, A. J.; Cammi, R.; Pomelli, C.; Ochterski, J. W.; Martin, R. L.; Morokuma, K.; Zakrzewski, V. G.; Voth, G. A.; Salvador, P.; Dannenberg, J. J.; Dapprich, S.; Daniels, A. D.; Farkas, O.; Foresman, J. B.; Ortiz, J. V.; Cioslowski, J.; Fox D. J., *Gaussian, Revision B.01*, 2010.
26. T. Lu and F. Chen, *J. Comput.Chem.*, 2012, **33**, 580.
27. S. Kakar, A. J. Nelson, R. Treusch, C. Heske, T. van Buuren, I. Jiménez, P. Pagoria and L. J. Terminello, *Phys. Rev. B*, 2000, **62**, 15666.
28. T. Y.-J. Han, P. F. Pagoria, A. E. Gash, A. Maiti, C. A. Orme, A. R. Mitchell and L. E. Fried, *New J. Chem.*, 2009, **33**, 50.
29. J. Yi, Y. Xiong, K. Cheng, M. Li, G. Chu, X. Pu and T. Xu, *Sci.Rep.*, 2016, **6**, 19364.
30. D. Polli, P. Altoe, O. Weingart, K. M. Spillane, C. Manzoni, D. Brida, G. Tomasello, G. Orlandi, P. Kukura, R. A. Mathies, M. Garavelli and G. Cerullo, *Nature*, 2010, **467**, 440.

31. S. Q. K. Cheng, J. Chen, *Chin. J. Energ. Mater.*, 2002, **10**, 13.
32. R. Hurley and A. C. Testa, *J. Am. Chem. Soc.*, 1966, **88**, 4330.
33. R. Hurley and A. C. Testa, *J. Am. Chem. Soc.*, 1968, **90**, 1949.
34. G. Chu, Z. Yang, J. Xin, T. Xi, Y. Zhao, W. He, M. Shui,Y. Gu, Y. Xiong, K. Cheng and T. Xu, *Submitted*.
35. R. A. Vogt and C. E. Crespo-Hernandez, *J. Phys.Chem. A*, 2013, **117**, 14100.
36. Y. Sun, Y. Shu, T. Xu, M. Shui, Z. Zhao, Y. Gu and X. Wang, *Cent. Eur. J. Energ. Mat.*, 2012, **9**, 411.

Table 1 Relative energy (eV) and Q_{nitro} (−e) values in different structures of TATB

Structure	State	Energy	Q_{nitro}			
			Site 1	Site 2	Site 3	Average
TA-S_0	S_0	0.00	0.397	0.397	0.397	0.397
	S_1	3.67	0.459	0.459	0.459	0.459
TA-S_1	S_0	0.40	0.389	0.392	0.392	0.391
	S_1	3.42	0.727	0.339	0.339	0.468
TA-S_1'	S_1	2.25	0.887	0.363	0.364	0.538
	T_1	2.43	0.645	0.375	0.372	0.464
TA-T_1	T_1	2.30	0.598	0.380	0.381	0.453

Figure captions

Fig. 1The structure of TATB in the S_0 state (TA-S_0), and the highest occupied molecular orbitals (HOMOs) and lowest unoccupied molecular orbitals (LUMOs).

Fig. 2. Total, partial, and overlap density-of-states (TDOS, PDOS, and OPDOS) for TATB.

Fig. 3 Measured and calculated steady-state absorption spectra of TATB in DMSO.

Fig. 4 a. Evolution-associated difference spectra (EADS) resulting from a global analysis of the transient absorption experiments on TATB. Dynamics traces recorded at b. 600 and c. 450 nm.

Fig. 5 (Upper) LUMO-4 and LUMO-6 of TA-S_0, together with (Lower) the geometrical structure, LUMO-1, LUMO-4, and LUMO-6 of TA-S_1.

Fig. 6 (Upper) Geometrical structure and LUMO-1 of TA-S_1', in which the dihedral C(4)C(5)N(10)O(12) twists to 69.7° and the dihedral C(6)C(5)N(10)O(11) twists to 104°. (Lower) Geometrical structure and HOMO-1 of TA-T_1, in which the dihedral C(4)C(5)N(10)O(12) twists to 46.9°, and the dihedral C(6)C(5)N(10)O(11) twists to 84.2°.

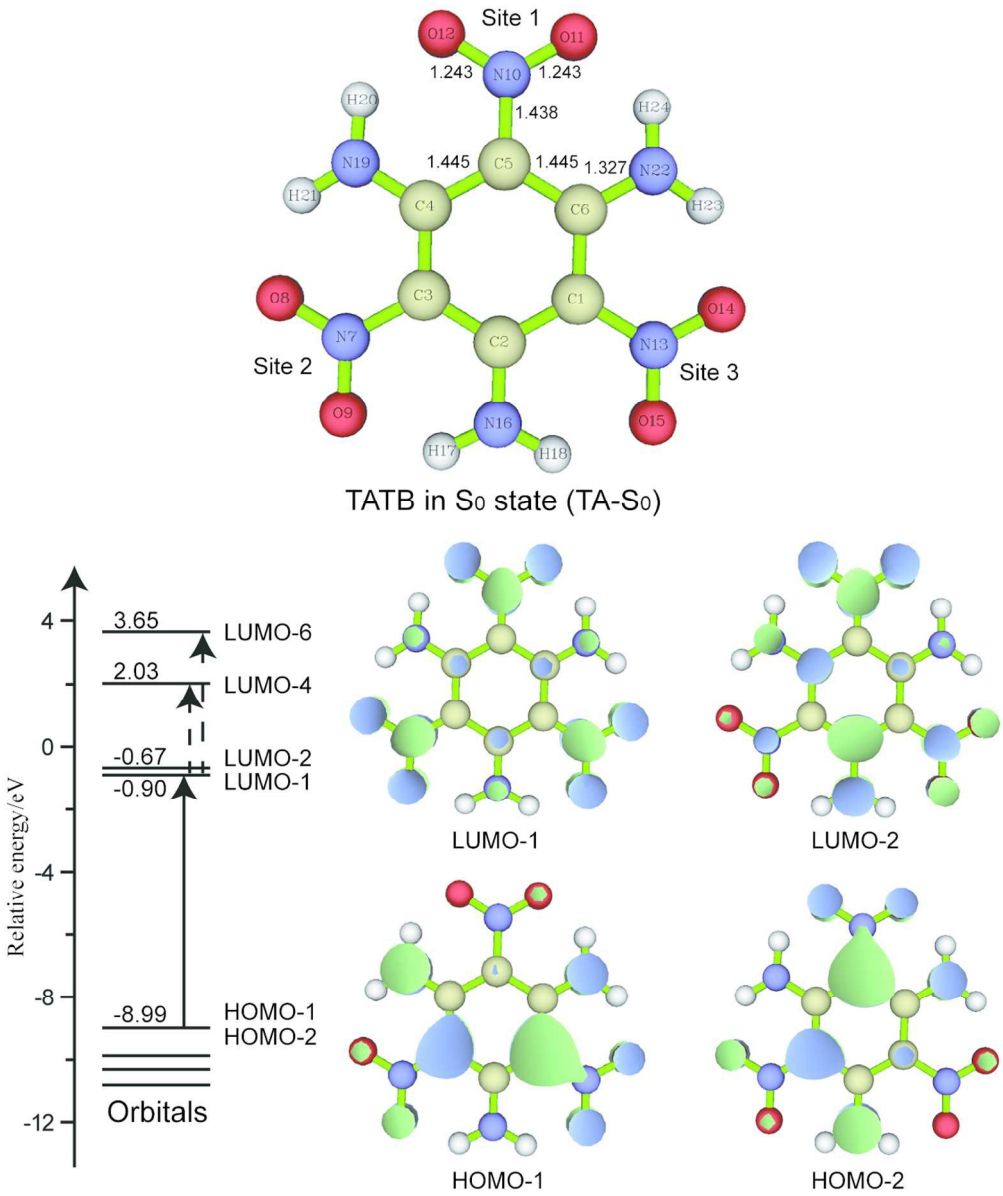

120x143mm (300 x 300 DPI)

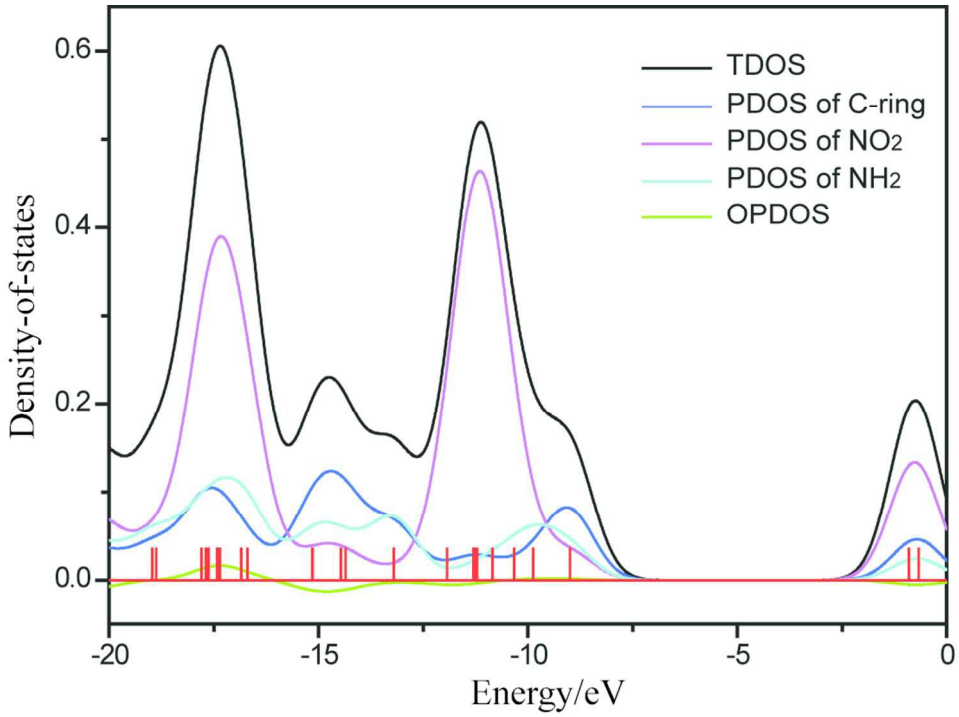

97x69mm (300 x 300 DPI)

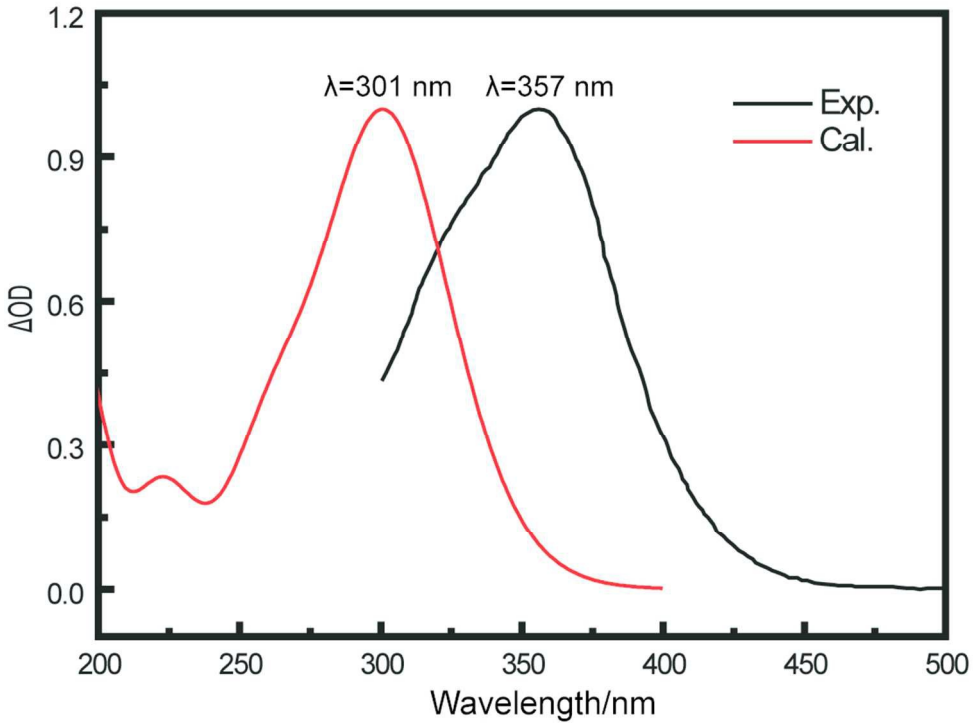

96x74mm (300 x 300 DPI)

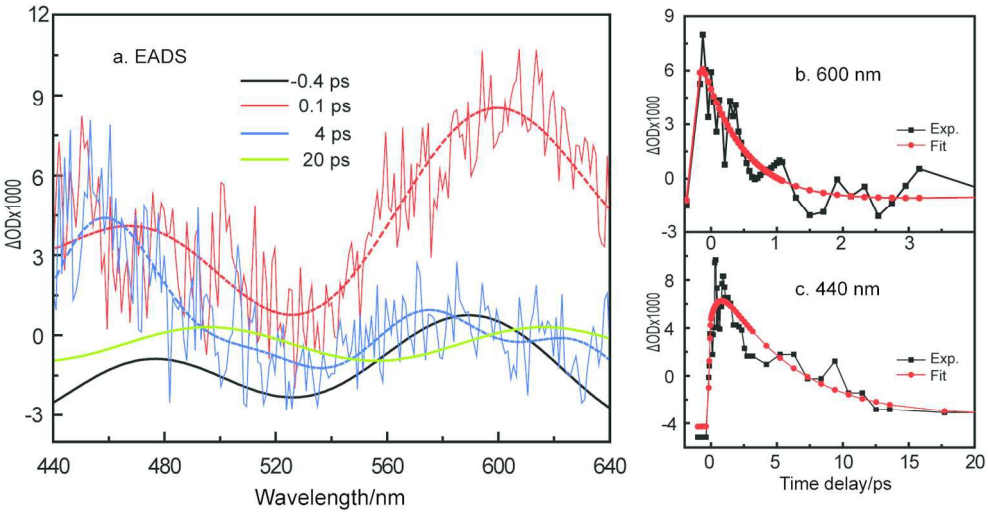

145x74mm (300 x 300 DPI)

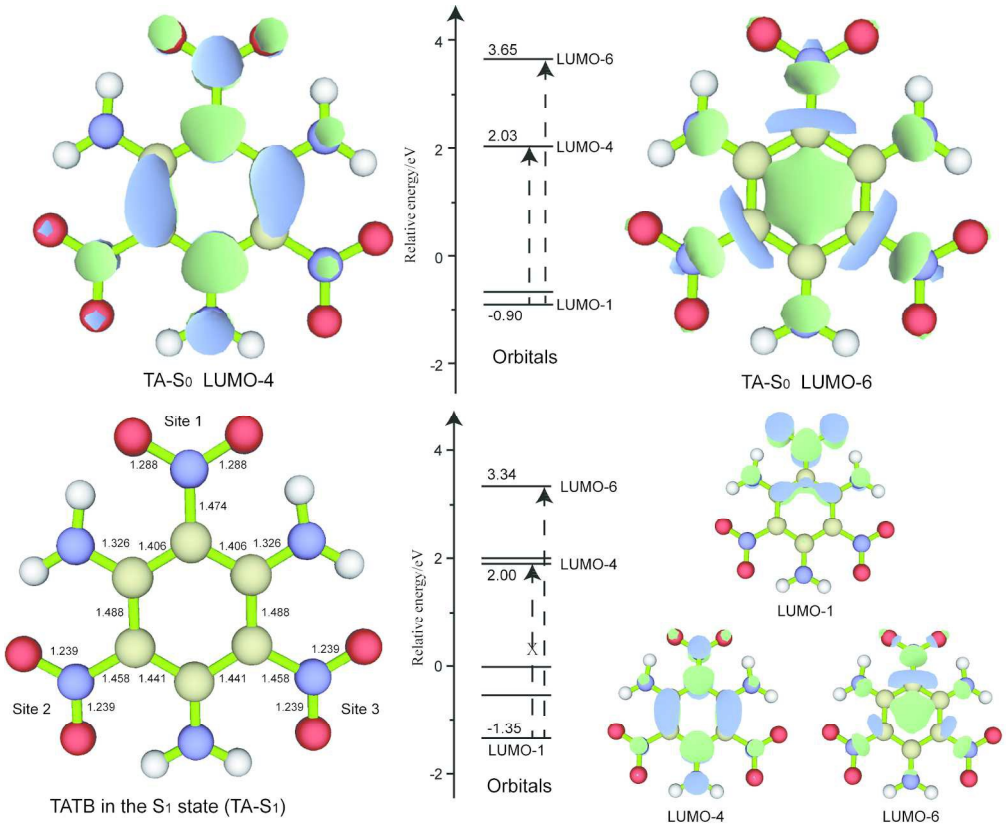

186x152mm (300 x 300 DPI)

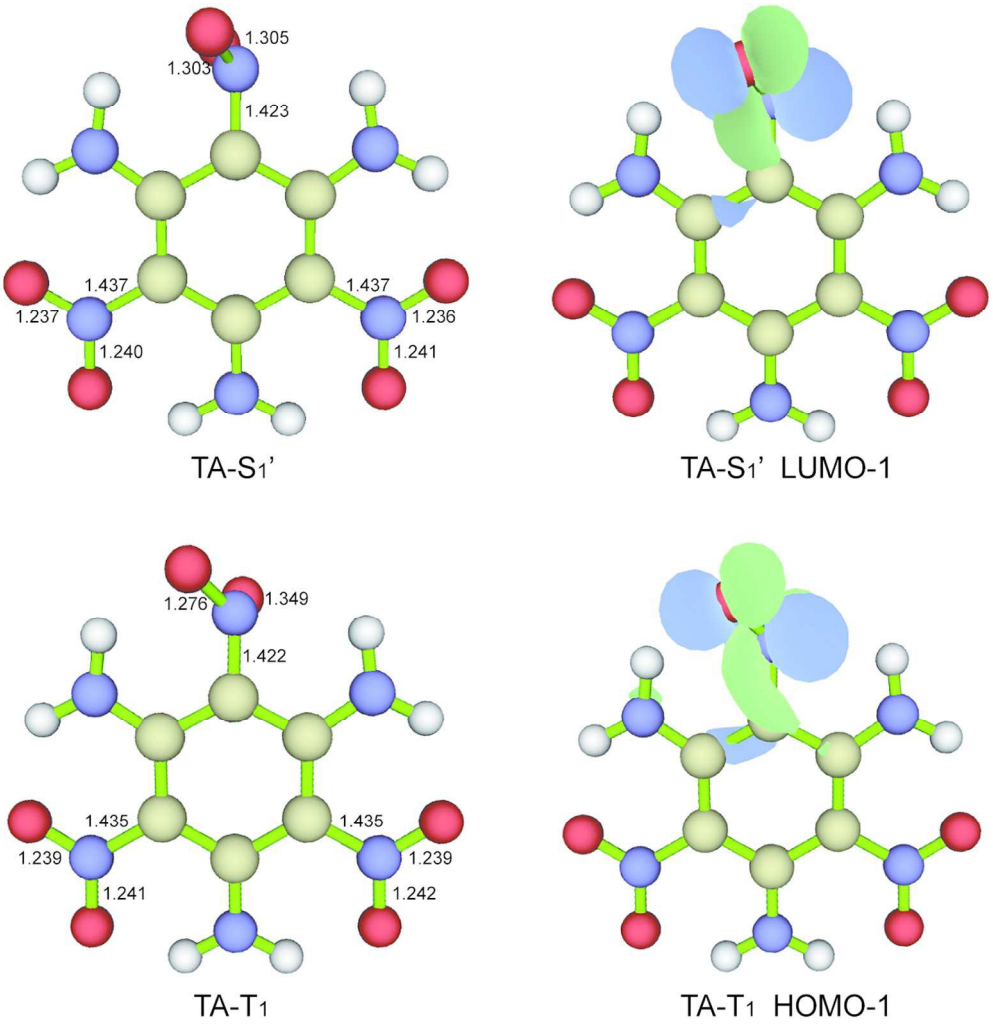

117x120mm (300 x 300 DPI)

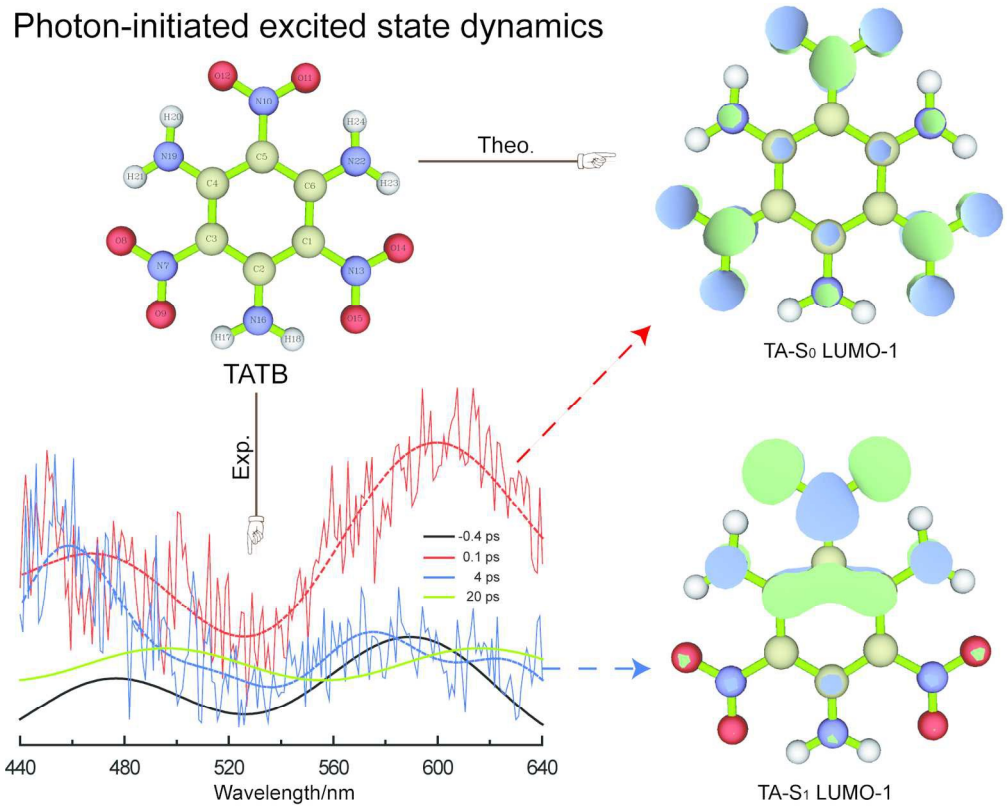

155x124mm (300 x 300 DPI)